Atmospheric
Chemistry
and Physics
Discussions

Local Time Dependence of Polar Mesospheric Clouds:
A model study

Francie Schmidt[1], Gerd Baumgarten[1], Uwe Berger[1], Jens Fiedler[1], and Franz-Josef Lübken[1]

[1]Leibniz-Institute of Atmospheric Physics, Rostock University, Kühlungsborn, Germany

Correspondence to: Gerd Baumgarten (baumgarten@iap-kborn.de)

Abstract.

The Mesospheric Ice Microphysics And tranSport model (MIMAS) is used to study local time (LT) variations of polar mesospheric clouds (PMC) in the northern hemisphere during the period from 1979 to 2013. We investigate the tidal behavior of brightness, altitude and occurrence frequency and find a good agreement between model and lidar observations. Mean ice water content (IWC) values from MIMAS also match those from satellite observations. In the latitudinal band of $67.5°$–$70.5°$N the IWC maximum throughout the day occurs at about 3 LT and the minimum around 18 LT with a ratio of maximum to minimum of 10. At the peak of the PMC layer the ice particle size varies by about 30 % while the median number density varies by a factor of 2 throughout the day. Furthermore, the absolute tidal variation of IWC generally increases towards higher latitudes and the time of maximum IWC changes from about 4 to 0 LT for latitudes from $63°$N to $81°$N. In the period from 1979 to 2013 we find an increase of the tidal amplitudes. The linear trend terms of diurnal and semidiurnal variations are calculated to be 3.4 and 1.4 g/km^2/dec. The persistent features of strong tidal modulations are caused by tidal structures in background parameters. The temperature varies by about 2 K and water vapor by about 3 ppmv at the altitude of ice particle sublimation near 81.5 km.

1 Introduction

Polar mesospheric clouds (PMC), also known as noctilucent clouds (NLC), consist of water-ice crystals. They occur at mid to high latitudes around 83 km altitude (e.g. Jesse, 1896; Gadsden and Schröder, 1998; Lübken et al., 2008). Such clouds form in summer in a supersaturated cold atmosphere with temperatures below 150 K and are sensitive to water vapor and mesospheric temperatures. Therefore, PMC are thought to be sensitive indicators of climate change in the middle atmosphere (e.g. Thomas, 1996; Berger and Lübken, 2015; Hervig et al., 2016). PMC often show a rich variability which provides information about thermal and dynamical processes on thermal background fields (Witt, 1962). The clouds have been shown to be subject to persistent local time variations (e.g. von Zahn et al., 1998; Chu et al., 2003; Fiedler et al., 2005). These variations were attributed to atmospheric thermal tides. Such tidal oscillations are globally forced due to absorption of solar irradiance throughout the day. While semidiurnal tides are dominantly generated through absorption of solar ultraviolet radiation by stratospheric ozone, water vapor in the troposphere absorbs solar radiation in the near-infrared bands forcing mainly the diurnal tidal component.

Generally, these tidal waves propagate upwards with exponential growth in amplitude, and are therefore also present at PMC altitudes in the summerly mesopause region at high latitudes.

A variety of spaceborne experiments have observed PMC since the late 20th century (e.g. Stevens et al., 2010; Russell et al., 2014; Hervig and Stevens, 2014). Many of these experiments are on satellites with sun-synchronous orbits and therefore

5 only allow observations at fixed local times. The Solar Backscattered Ultraviolet Instruments (SBUV) on-board the National Oceanic and Atmospheric Administration (NOAA) satellites provide a data set of more than 35 years of PMC observations (e.g. Thomas et al., 1991). This data set was recorded by eight separate instruments with changing viewing conditions and different local times which introduces uncertainties in the long-term analysis when creating a single data set. Also the Solar Occultation For Ice Experiment (SOFIE) and the Cloud Imaging and Particle Size (CIPS) instrument on-board the Aeronomy

10 of Ice in the Mesosphere (AIM) satellite perform observations in a sun-synchronous orbit. The Ozone Monitoring Instrument (OMI) on-board the Aura satellite is able to measure PMC at different local times, but only part of the diurnal cycle is covered, i.e. the afternoon is missing (DeLand et al., 2011). In order to quantify long-term natural or anthropogenic changes in PMC, it is therefore essential to understand their variations over the diurnal cycle (DeLand and Thomas, 2015). Observations from satellites apparently have a limited ability to directly characterize local time effects on global scales.

15 Opposite to satellites, ground-based measurements have the ability to cover a full local time cycle. E.g. variations of PMC occurrence frequency and brightness as function of local time have been observed in detail with lidar instruments (von Zahn et al., 1998; Chu et al., 2006; Fiedler et al., 2005, 2009, 2011, 2016; Gerding et al., 2013). All these data show evidence of a large PMC brightness variability with local time.

In this paper we discuss results from a three-dimensional Lagrangian transport model for PMC called MIMAS (Mesospheric

20 Ice Microphysics And tranSport model). MIMAS covers the latitude and altitude range of PMC and the entire PMC season with a high temporal resolution. This allows for example to calculate latitude-dependent local time adjustments to retrieve PMC parameters with the observational filter of satellite instruments. In the next section we describe some important aspects of the MIMAS model which are relevant for the simulation of seasonal and local time variations in PMC. Sections 3 and 4 give an overview of seasonal and local time variations seen in MIMAS and compared to observations of PMC. In section 5 we

25 characterize local time variations of the background atmosphere as calculated by the model. Finally, we discuss the latitude dependence and year-to-year changes of PMC local time variations and their implications for the analysis of long-term changes.

2 Model description

The MIMAS model is a 3-dimensional Lagrangian transport model designed specifically to model ice particles in the meso-sphere/lower thermosphere (MLT) region. MIMAS is limited to mid and high latitudes ($45-90°$N) with a horizontal grid of

30 $1°$ in latitude and $3°$ in longitude, and a vertical resolution of $100\,\mathrm{m}$ from 77.8 to 94.1 km (163 levels).

Typically, MIMAS calculates a complete PMC season from mid of May to end of August. Each of the seasonal simulations starts with same water vapor distributions on constant pressure levels (Berger and Lübken, 2015). Then, the background water

vapor is transported by 3-d winds, mixed by turbulent diffusion, and reduced by photo-dissociation from solar ultraviolet radiation. We use Lyman-α as a proxy for solar activity (available at http://lasp.colorado.edu/lisird/lya/).

Simultaneously, 40 million condensation nuclei (dust particles) are transported according to 3–d background winds, particle eddy diffusion, and sedimentation. The radii of the dust particles in the model vary according to a Hunten distribution between
5   1.2 and 3.6 nm (Berger and von Zahn, 2007). While each of the 40 million particles is transported on an individual 3–d trajectory with a time step of 45 s, a single dust particle will nucleate or an already existing ice particle will further grow, respectively, whenever the temperature and water vapor concentration of the background atmosphere provide conditions of supersaturation. In case of undersaturated conditions a preexisting ice particle will start to sublimate. The local formation, growth, and sublimation of all ice particles are interactively coupled to the local background water vapor concentration which
10   leads to a redistribution of H_2O with local freeze drying and water supply (von Zahn and Berger, 2003; Kiliani, 2014; Berger and Lübken, 2015).

In MIMAS temperatures, densities, pressure and wind fields are prescribed using hourly output data from the Leibniz Institute Middle Atmosphere (LIMA) model which especially aims to represent the thermal structure around mesopause altitudes (Berger, 2008). LIMA is a fully nonlinear, global, and three-dimensional Eulerian grid point model taking into account major
15   processes of radiation, chemistry, and transport. LIMA extends from the ground to the lower thermosphere (0–150 km), and applies a triangular horizontal grid structure with 41804 grid points in every horizontal layer ($\Delta x \approx \Delta y \approx 110$ km). This allows to resolve the fraction of the large-scale internal gravity waves with horizontal wavelengths of ≥ 500 km.

LIMA is nudged to tropospheric and stratospheric reanalysis data available from the European Centre for Medium-Range Weather Forecasts (ECMWF), Reading, United Kingdom. LIMA incorporates the 40 year ECMWF reanalysis data set (ERA-
20   40) from 1960 to 2002 and ECMWF operational analysis thereafter. The nudging coefficient is altitude dependent with a constant value of $1/3.5$ days^{-1} from the ground to the middle stratosphere (35 km). Above 35 km, the coefficient linearly decreases to zero until 45 km. The nudging of ECMWF data introduces short-term and year-to-year variability. Above approximately 40 km, carbon dioxide and ozone concentrations as well as solar activity vary with time. For CO_2 we have used a monthly mean time series for the entire period (1961–2013) as measured at Mauna Loa (from http://www.esrl.noaa.gov/gmd/ccgg/trends).
25   For ozone, we take a temporal variation in the height region of the upper stratosphere and lower mesosphere (40–65 km) into account. More precisely, we have used relative anomalies at 0.5 hPa from 1979 to 2013 as measured by SBUV satellite instruments (from http://acd-ext.gsfc.nasa.gov/Data-services/merged/), for more details see Lübken et al. (2013). Before 1979 ozone data are taken from the World Meteorological Organization (WMO) report. Finally, daily Lyman-α fluxes from January 1961 until December 2013 are taken as a proxy for solar activity.

30   ## 3   Seasonal variations

During the northern hemispheric summer PMC typically occur from end of May until mid of August (e.g. Thomas and Olivero, 1989; Gadsden and Schröder, 1998; Hartogh et al., 2010; Hervig et al., 2013). At the core of the ice season in July, lowest
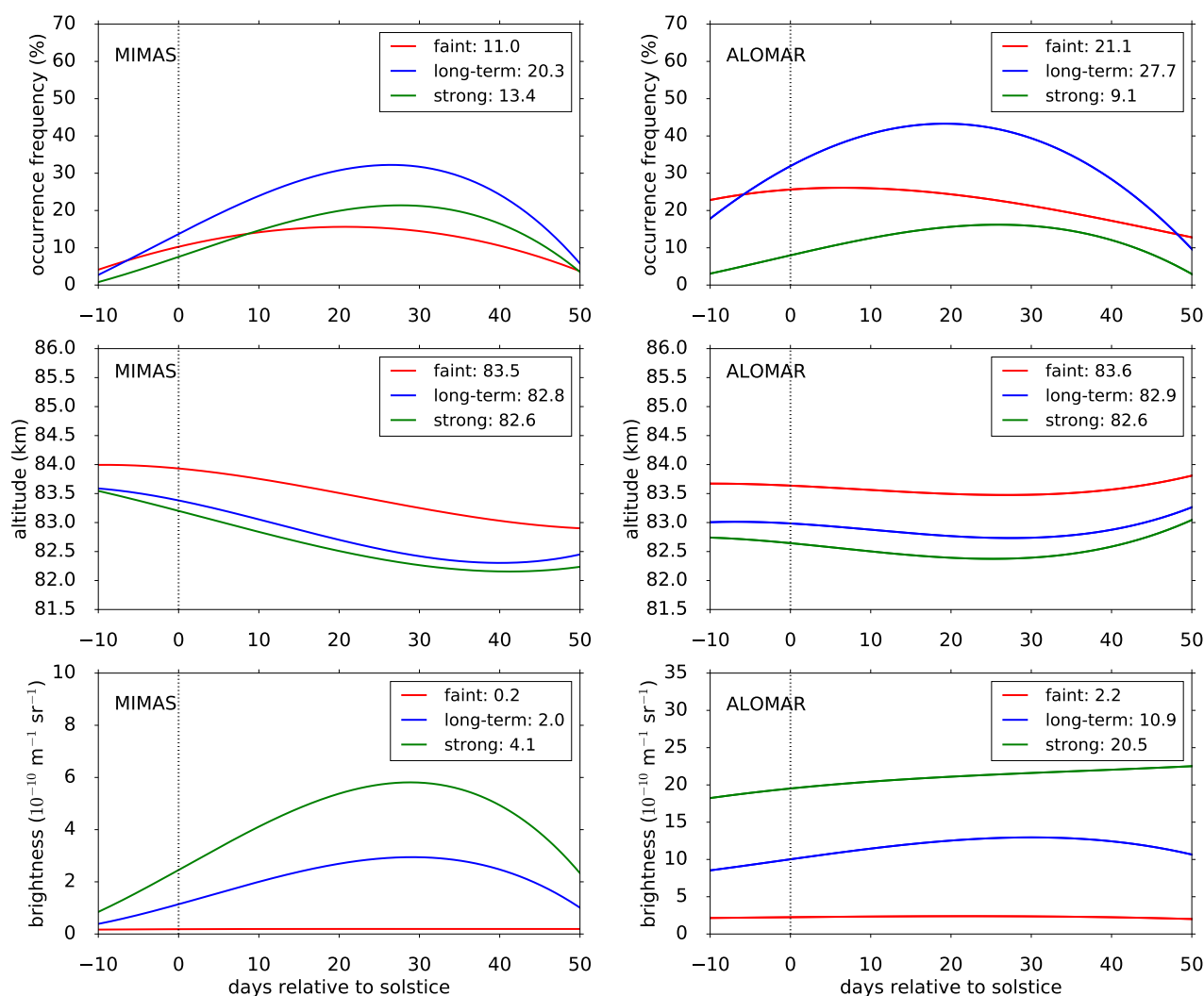
Atmospheric
Chemistry
and Physics
Discussions

Figure 1. Mean seasonal variations of PMC occurrence frequency (upper panel), altitude (middle panel) and brightness β_{max} (lower panel) between 2003 and 2013 at ALOMAR for faint (red), long-term (blue) and strong (green) clouds (for details see text). Left panels show model data for $67.5 - 70.5°N$, $10.5 - 19.5°E$, right panels show lidar observations from ALOMAR. The solid lines represent third-order polynomial fits based on daily means. Numbers in the Figure legends are seasonal mean values. Brightness ranges for cloud classes are scaled down by a factor of 4 for MIMAS data. Note the different scaling of the brightness axis for model and lidar data.

Atmospheric
Chemistry
and Physics
Discussions

temperatures near $130\,\mathrm{K}$ have been observed at mesopause altitudes near $88\,\mathrm{km}$ at $69°\mathrm{N}$ (Lübken, 1999). Hence, we expect PMC most frequently and bright during July.

Figure 1 shows the mean seasonal variations of basic PMC parameters as calculated by MIMAS and observed by the Rayleigh/Mie/Raman(RMR)-lidar at the Arctic Lidar Observatory for Middle Atmosphere Research (ALOMAR), located at
5 $69°\mathrm{N}$, $16°\mathrm{E}$ (Fiedler et al., 2016). MIMAS data are limited to a latitudinal and longitudinal area of $67.5 - 70.5°\mathrm{N}$ and $10.5 - 19.5°\mathrm{E}$ to be close to the lidar position. We will use the volume backscatter coefficient of ice particles $\beta_{\max}$, in units of $10^{-10}\,\mathrm{m}^{-1}\mathrm{sr}^{-1}$, as a measure for the cloud brightness. Both, model and observations cover the same time period of 11 years from 2003 to 2013. In order to take different cloud classes and the detection sensitivity of the lidar into account, we sort measurements and model data into different brightness ranges: $1 < \beta_{\max} < 4$ (faint clouds), $\beta_{\max} > 4$ (long-term detection
10 limit of the lidar), and $\beta_{\max} > 13$ (strong clouds) (e.g. Fiedler et al., 2003; Baumgarten et al., 2008).

In order to convert the model output from MIMAS to specific lidar measurements, we apply spherical Mie-theory calculations to modeled ice particle distributions while taking into account the laser wavelength ($532\,\mathrm{nm}$) and scatter geometry ($180°$). Finally, the transformed model data are sorted into brightness ranges. PMC brightness is proportional to the number of ice particles and depends approximately by the power of six on ice particle radius. For example, increasing the mean radius
15 by only $25\,\%$ from $32\,\mathrm{nm}$ to $40\,\mathrm{nm}$ would result into a brightness change by a factor of 4. It is this high sensitivity of cloud brightness to particle size that forms a hard benchmark for our complex ice model simulations. A small underestimation of the mean ice radius will dramatically decrease the brightness, on the other hand, a small overestimation will enhance the resulting backscatter signal by orders of magnitude. In order to match the mean occurrence frequencies of the lidar measurements we decreased the brightness ranges, defining the cloud classes, for the model data by a scaling factor of 4. Hence, the modeled
20 occurrence frequencies contain a systematic bias. We think this deficiency is tolerable since our local time analysis relates to relative deviations from a mean. The scaling factor will only be used for the comparisons with lidar data in this and the following section.

The upper panels of Figure 1 show a general good agreement of modeled and observed PMC occurrence frequencies. We find maximum values in the long-term and strong cloud classes in mid July around days relative to solstice (DRS) $20 - 30$.
25 Faint clouds observed by lidar occur earlier in the season than modeled faint clouds. This gives a hint that the model perhaps underestimates the microphysical process of nucleation in ice formation which essentially determines the frequency of weak PMC consisting of small ice particles. We note that ice nucleation in MIMAS is described by the concept of critical radius (Turco et al., 1982; Berger and von Zahn, 2002; Berger and Lübken, 2015).

The middle panels of Figure 1 show modeled and observed PMC altitudes which coincide quite well. Generally, weak PMC
30 are at higher altitudes compared to strong PMC. This altitude separation is caused by two reasons. First, the sedimentation velocities of ice particles depend on their sizes. Weak PMC consist of ice particle distributions with smaller mean radii, typically in a range of $20\,\mathrm{nm}$, whereas strong PMC consist of larger mean radii, e.g. $40\,\mathrm{nm}$. As the sedimentation velocity increases with particle size (mass), larger particles can reach lower altitudes along their sedimentation path. Secondly, smaller ice particles start to sublimate at lower temperatures than larger ones due to the Kelvin effect. Thus, the negative vertical

Atmospheric
Chemistry
and Physics
Discussions

Open Access

temperature gradient of the atmosphere causes smaller particles to sublimate at higher altitudes than larger particles. As a result larger ice particles, causing a higher brightness, are found at lower altitudes.

The lower panels of Figure 1 show modeled and observed PMC brightness. Here, the model data are calculated according to a given brightness range as an arithmetic mean of all brightness values matching the limits. Again, the model seems to
5 underestimate begin and end of the season. The scaling factor for the brightness ranges leads to lower modeled brightness values in the different cloud classes. Hence, multiplying the modeled values with the scaling factor of 4 approximately reproduces the brightness values observed by lidar.

We summarize that the modeled seasonal distributions of occurrence, altitude and brightness are fairly consistent with the ALOMAR RMR-lidar observations, especially for July conditions. Therefore we will concentrate our discussion of model
10 results in the following sections on this core period of the northern PMC season.

4 Local time variations

PMC preferentially occur during morning hours which is attributed to thermal tides of background temperatures in the mesopause region (Fiedler et al., 2011). In order to validate the structure of local time variations in MIMAS we compare our model data to observations by the RMR-lidar at ALOMAR and to instruments on-board the AIM satellite. For comparison to lidar data we
15 will apply a scaling factor of 4 regarding the brightness ranges, defining the cloud classes, as described in the previous section. As discussed above we will concentrate on the core period of the northern PMC season and will use only July data (31 days x 24 h) from MIMAS simulations for the PMC seasons 2003 – 2013. Tidal structures in the LIMA model have been discussed earlier by Herbort et al. (2007) and Fiedler et al. (2011).

4.1 Occurrence frequency, altitude, and brightness

20 Figure 2 shows the variation of PMC occurrence frequency, altitude, and brightness throughout the day for the integrated data set of July 2003 – 2013 and brightness classes as defined above. The curves are superpositions of four harmonic functions with periods of 24, 12, 8, and 6 h, which are fitted to hourly mean values as described in Fiedler et al. (2016). The geographic range is again restricted to the area around ALOMAR. We find pronounced and persistent features which indicate a strong influence of tides on PMC parameters. The occurrence frequency variation over a day is largest for strong clouds both in
25 MIMAS and observations. Like in the observations, the model results show highest cloud occurrence during the morning hours. The local time dependencies of altitude and brightness are anti-correlated, i.e. on average ice clouds of higher brightness are found at lower altitudes. In general, a predominant diurnal oscillation exists in agreement with the lidar observations. The lidar observations show additionally semidiurnal variations in all three PMC parameters, which seems to some extent underestimated by the model. Contrary, the modeled brightness shows a clear peak in the morning hours around 4:00 LT which
30 is absent in the observations.

In order to investigate these different structures we calculated the ratios of diurnal to semidiurnal tidal amplitudes (A_{24}/A_{12}). The values in Table 1 show that both model and lidar fits have nearly the same amplitude ratios for a number of cloud parameter
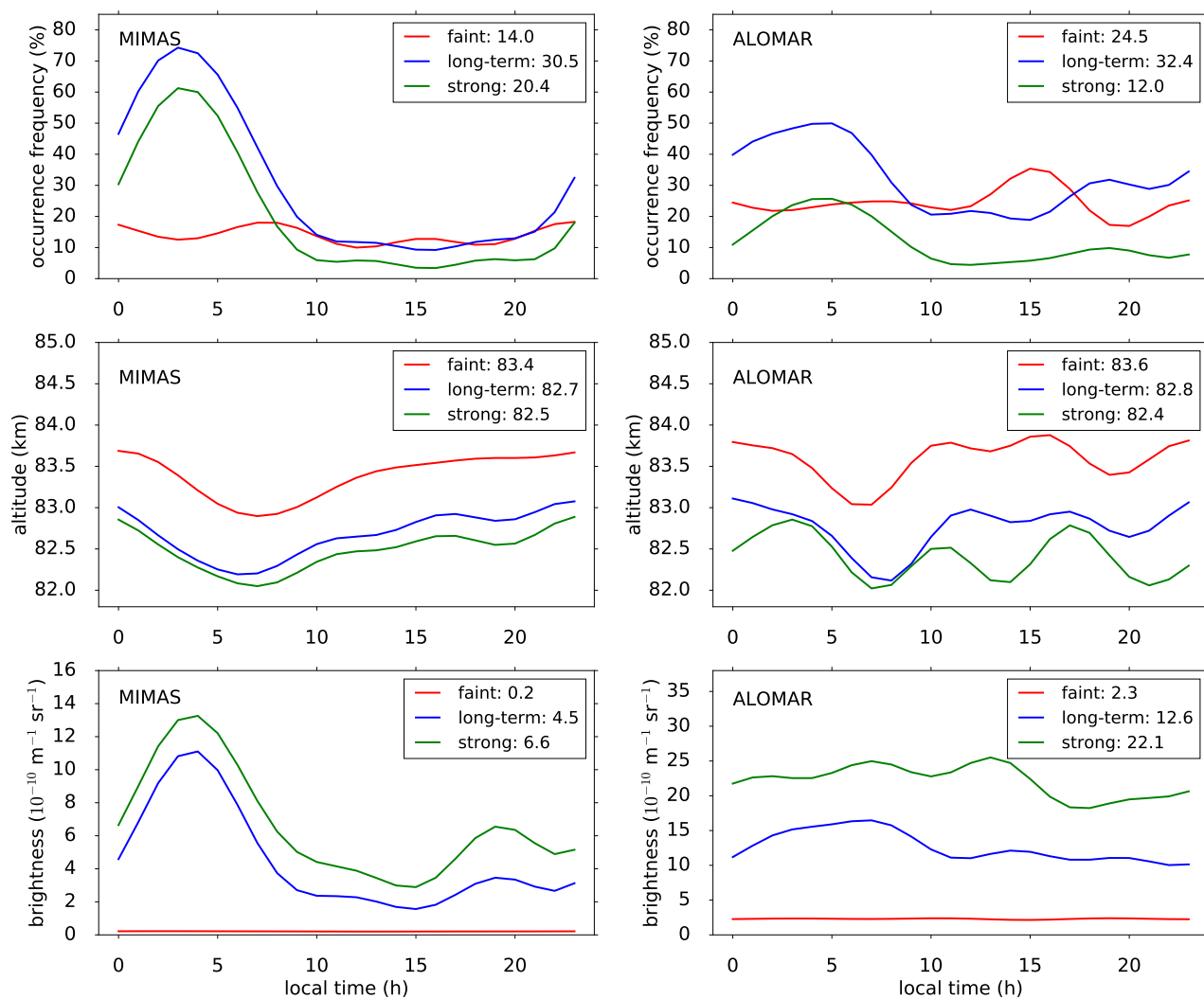
Atmospheric
Chemistry
and Physics
Discussions

Figure 2. Mean local time variations of PMC occurrence frequency (upper panel), altitude (middle panel) and brightness β_{max} (lower panel) for July in the period from 2003 to 2013 at ALOMAR for faint (red), long-term (blue) and strong (green) clouds (for details see text). Left panels show model data for $67.5 - 70.5°$N, $10.5 - 19.5°$E, right panels show lidar observations from ALOMAR. The lines represent the sum of four harmonic fits using periods of 24, 12, 8, and 6 h to hourly mean values. Numbers in the Figure legends are daily mean values. Brightness ranges for cloud classes are scaled down by a factor of 4 for MIMAS data. Note the different scaling of the brightness axis for model and lidar data.

and class combinations. For example, for the long-term brightness the ratios are 1.82 (model) and 1.88 (lidar), meaning that tidal modes are very similar in both data sets. Thus the phase differences of modeled and observed data, especially for the semidiurnal modes, (not shown here) are mostly responsible for the differences visible in Figure 2. The superposition of diurnal and semidiurnal tidal modes yields a stronger morning peak in the modeled compared to the observed brightness.

5   In summary, observed local time variations of PMC occurrence and brightness at ALOMAR are fairly well reproduced by MIMAS.

	MIMAS			RMR-lidar		
	OF	altitude	brightness	OF	altitude	brightness
faint	1.40	2.25	5.71	0.89	0.67	0.71
long-term	**2.45**	2.36	**1.82**	**2.51**	0.77	**1.88**
strong	**2.00**	1.75	**1.96**	**1.59**	3.02	**2.44**

Table 1. Ratio of diurnal to semidiurnal amplitudes (A_{24}/A_{12}) of harmonic fits to the modeled and observed occurrence frequency (OF), altitude, and brightness. The values are calculated for different cloud classes (for details see text) for July months in the period from 2003 to 2013 at ALOMAR according to Figure 2. Bold numbers mark values that agree within the relative uncertainty of about 15 % (confidence level of 95 %).

4.2   Ice Water Content

Comparison of PMC brightness values between different instruments is affected by observational constraints, e.g. viewing geometry, lighting conditions, temporal overlap and wavelength. Stevens et al. (2005) suggested that integrated ice mass has

10   the advantage to be less dependent on instrumental setups and thus should be more robust to be used for PMC comparisons. Therefore we present in this section model results of ice water content (IWC) which are calculated from the integrated ice mass density over the total vertical ice column. We analyze the time period $2007-2013$ to cover the time range of the SOFIE instrument on-board the AIM satellite. The IWC is calculated from all longitudes in the latitude band $67.5-70.5°$N. In order to resolve tidal structures we subdivide each latitudinal circle into 120 longitudinal segments and sort the model data according

15   to actual local times at all segments. This method yields a total of 3 latitudes times 120 longitudes times 31 days times 24 h of values for July conditions. Finally, we average all IWC values corresponding to a certain local time with a local time resolution of one hour per day. The probability density distributions of all these IWC values show to a high degree an exponential behavior. Therefore we calculate two different averages (median and arithmetic mean), in order to characterize a mean ice water content as a function of local time during July.

20   In Figure 3 we compare our IWC model results in terms of median values with measurements from the CIPS and SOFIE instruments on-board the AIM satellite for the latitude band $67.5-70.5°$N. The AIM satellite operates in a sun-synchronous orbit, hence only limited local times are available (Russell et al., 2009). For comparison with model data we take the different sensitivities of the two AIM instruments (SOFIE, CIPS) into account. The detection threshold for SOFIE is given as 0.5 g/km^2
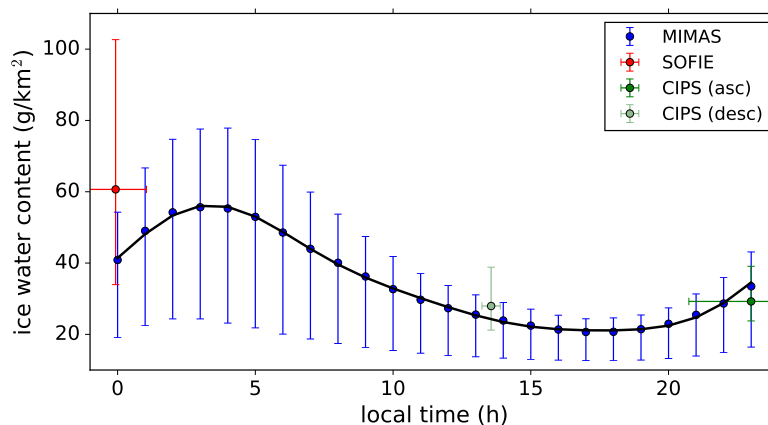
Atmospheric
Chemistry
and Physics
Discussions

Figure 3. Hourly median values of IWC from $2007 - 2013$ (July) for $67.5 - 70.5°$N and IWC threshold of $10\,g/km^2$ as a function of solar local time. The vertical bars represent the lower and upper quartile of the data. The black curve is a harmonic fit to the data with periods of 24, 12, and 8 h. Data from AIM satellite instruments including uncertainties for the same time range: SOFIE V1.3 (red - from http://sofie.gats-inc.com/sofie/index.php) and CIPS Level 3c (green - from http://lasp.colorado.edu/aim/download-data-pmc.php) for ascending and descending nodes.

(Hervig et al., 2009a). In contrast to SOFIE, the CIPS instrument is less sensitive allowing only IWC events larger than $10\,g/km^2$ to be detectable (Lumpe et al., 2013). Hence all IWC datasets (MIMAS, SOFIE, CIPS) are limited to this threshold. We find a good agreement between model results and the data points from SOFIE and CIPS inside the error bars. Generally, the modeled IWC has maximum values in the early morning hours between 1 and 4 LT and lowest values between 16 and 20 LT.

5 On average the IWC varies by a factor of about two during a day. Interestingly, comparing SOFIE with CIPS data, the CIPS observation at 23:00 LT does not match the SOFIE point for midnight conditions. There is a substantial deviation between these values of (SOFIE: $60\,g/km^2$i, CIPS: $30\,g/km^2$) which might be due to some uncertainties in the CIPS threshold. The MIMAS value of $40\,g/km^2$ is right in between the two different satellite observations. Nevertheless, all three data points coincide within their error bars.

10 We summarize that the MIMAS model results of PMC ice water content are compatible to a high degree with the satellite observations.

Figure 4 shows again the IWC local time variation for the latitude band $67.5 - 70.5°$N, but without any threshold which means that IWC values of zero (no PMC) are included. This yields an IWC variation over day by a factor of ten compared to the factor two when considering the threshold used in Figure 3. Hence, the strength of local time variations is sensitive to the

15 IWC threshold, meaning that larger thresholds induce smaller local time variations. The times of IWC maxima and minima are close to those of occurrence frequency and the brightness as shown in Figure 2. We find the harmonic fit to be highly correlated to the median values (correlation coefficient of 0.99), meaning that the local time behavior of IWC medians is almost perfectly
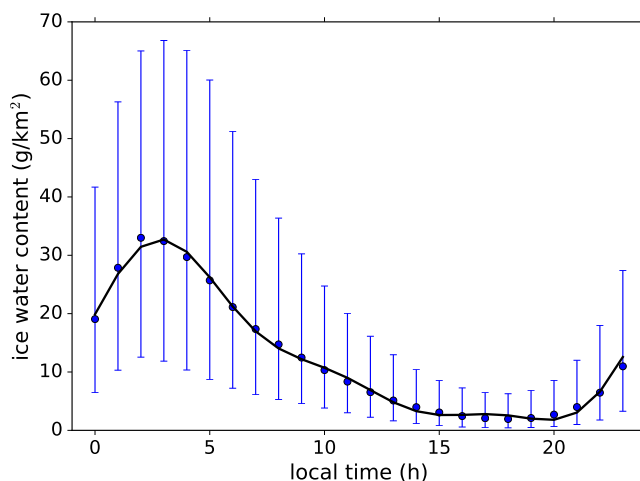
Atmospheric
Chemistry
and Physics
Discussions

Figure 4. Hourly median values of IWC from 2007–2013 (July) for 67.5–70.5°N as a function of solar local time. The vertical bars represent the lower and upper quartile of the data. The black curve is a harmonic fit to the data with periods of 24, 12, and 8 h.

represented by the three harmonics of 24, 12, and 8 hours. The fit is dominated by the diurnal mode, the amplitude ratios are $A_{24}/A_{12} = 2.66$ and $A_{24}/A_8 = 5.84$.

5 Influence of atmospheric background conditions on the local time behavior of ice particles

In the previous sections we compared MIMAS simulations with observations in order to show that MIMAS provides realistic
5 model results. Now we investigate local time variations in ice parameters and the background atmosphere as calculated by MIMAS and LIMA to find out the underlying reasons for the observed variations.

5.1 Ice particle parameters

Our model simulations of PMC show that the number of ice particles is largest at mesopause altitudes between 86 and 89 km where the highest chance of nucleation is found. This altitude region serves as a reservoir of small ice particles. Due to
10 random diffusive transport processes a fraction of these small ice particles experiences enhanced growing. The increase in particle mass enhances downward sedimentation. Towards lower altitudes the amount of free background water molecules increases exponentially since air density increases exponentially. During their downward sedimentation path the growth of ice is stimulated until an ice particle reaches an altitude where supersaturated background conditions change into undersaturation. This is the height where the radius of ice particles maximizes and thus highest ice mass densities and largest backscatter signals
15 occur.

In Figure 5 we present mean ice radius, number density, brightness, and ice mass density at the altitude of maximum backscatter signal for the latitude band 67.5–70.5°N during July. The plots show both median and arithmetic mean values.

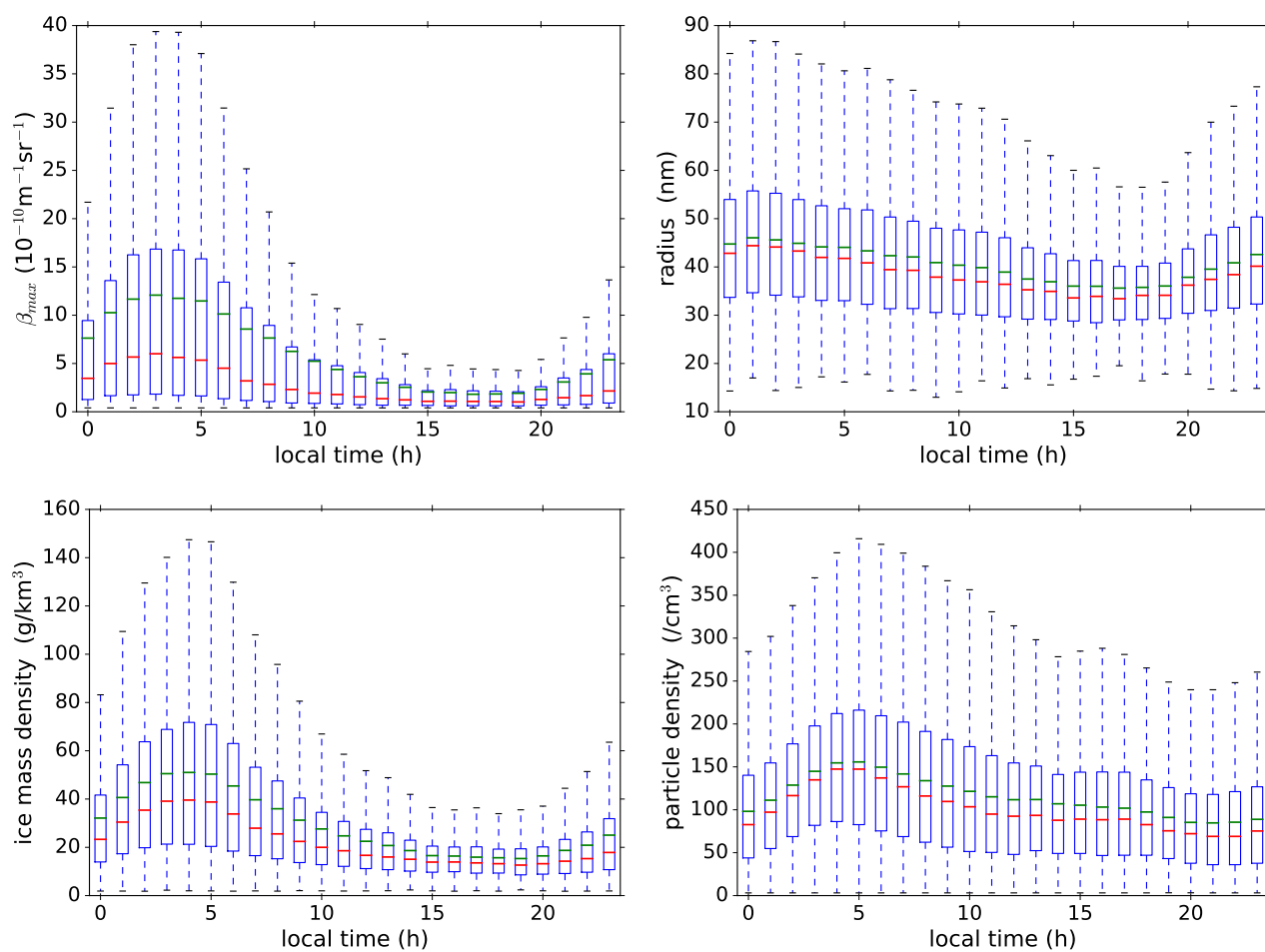Atmospheric
Chemistry
and Physics
Discussions

Figure 5. Ice parameters at $67.5 - 70.5°$N calculated from MIMAS simulations of all July months $2003 - 2013$ for the altitude range where $\beta_{\max} > 0.4$. Upper panels: brightness and ice particle radius. Lower panels: ice mass density and particle number density. The boxes represent lower and the upper quartiles, median (red line), and arithmetic mean (green line). The dashed vertical bars indicate the minimum and maximum values.
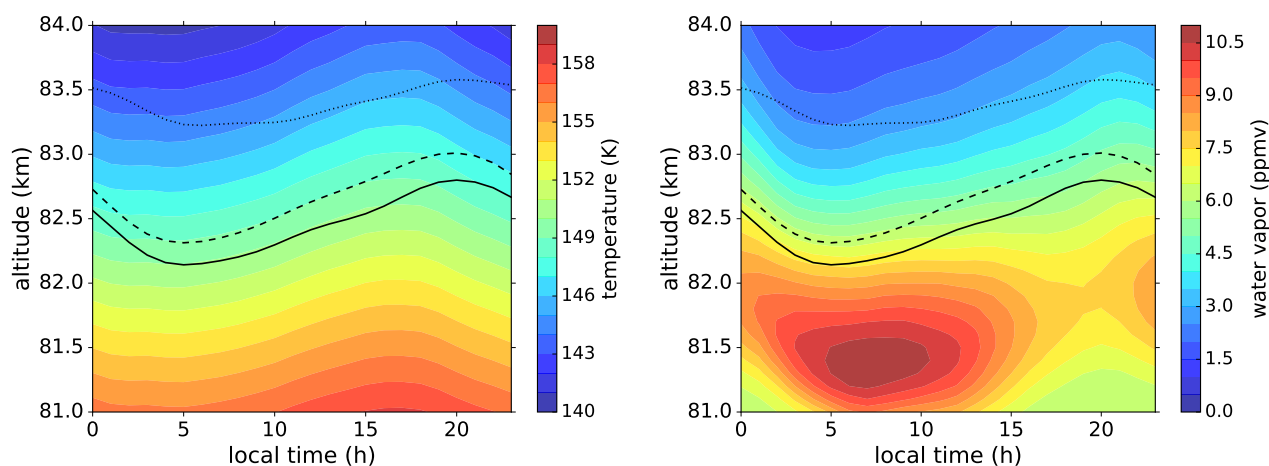
Atmospheric
Chemistry
and Physics
Discussions

Figure 6. Hourly mean values of temperature (left) and water vapor (right) in the latitude band $67.5 - 70.5°$N for July 2009. The black lines correspond to the mean altitudes of β_{max} for different cloud brightness classes: Strong (solid line), long-term (dashed line), and faint clouds (dotted line).

Median and arithmetic mean are generally different which indicates that the underlying distributions are not symmetric. We also find that the ice number density maximizes in the morning hours between 3 and 5 LT, which corresponds with the maxima of ice mass density and β_{max}. The mean radius shows a smaller variation with local time and no pronounced maximum during in the morning. This indicates that the local time behavior of ice mass density is mainly determined by the number of ice
5   particles and less by the ice particle radius. Our model results are confirmed by AIM observations which show that an increase in ice mass is significantly correlated with increasing number densities and less correlated with the size of ice particles (Hervig et al., 2009b). It is interesting to note that model calculations performed with the 1–d ice model CARMA show controversial results, meaning that particle number density has no effect on ice mass and brightness (Megner, 2011).

5.2   Atmospheric background conditions

10   In MIMAS local time dependencies in ice formation are mainly forced by tidal variations in background temperature and water vapor. Figure 6 shows these parameters on geometric altitudes in the latitude band $67.5 - 70.5°$N for July 2009. We selected a single year to be unaffected by possible long-term variations of the local time behaviour and have chosen season 2009 from the available years (1979 – 2013) because MIMAS model results show particular strong tidal effects on PMC during this year. In addition, the year 2009 was analyzed in detail by previous studies (Kiliani et al., 2013; Kiliani et al., 2015).
15   First of all we find that both background temperatures and water vapor have a pronounced tidal component. Furthermore, PMC altitudes of strong, long-term and faint cloud classes show variations of about 0.5 km with local time. Generally, bright PMC are found at lowest altitudes and follow nicely the temperature structure in the course of the diurnal cycle. Faint clouds are located about 1 km higher compared to strong clouds. The local time behavior of water vapor shows a pronounced maximum
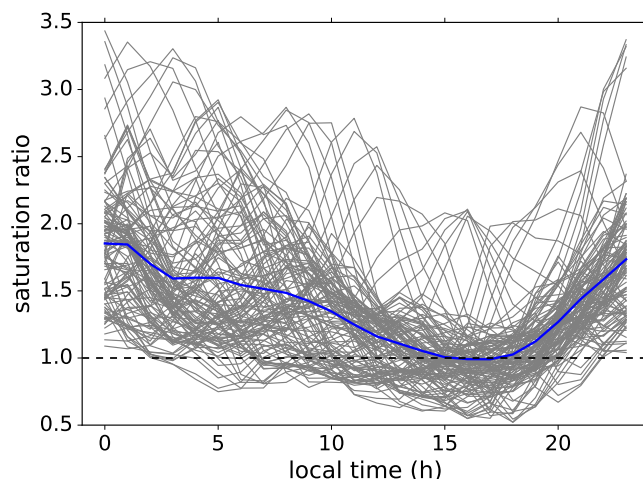
Atmospheric
Chemistry
and Physics
Discussions

Figure 7. Hourly mean values of the saturation ratio ($S \cong p_{H_2O}/p_{sat}$) in the latitude band $67.5 - 70.5°$N for July 2009 at a fixed altitude of 82.7 km as function of local time, taking into account the Kelvin effect. Grey lines show individual days and the blue line their mean.

during the morning. We find the maximum water vapor to occur between 5 and 10 LT and hence about 4 hours after the brightness maximum, cf. Figure 5. However, the minima of water vapor and β_{max} in the evening seem to match somewhat better. At the altitude of strong clouds temperature varies by about 2 K and water vapor by about 2 ppmv throughout the day. Around 81.5 km, which is roughly the altitude of sublimation, the variations are 2 K and 3 ppmv between minimum and
5 maximum.

Saturation conditions are a combined effect of temperature, water vapor, ambient pressure and particle radius. Figure 7 shows the saturation ratio S at a fixed altitude of 82.7 km, which is the mean PMC altitude in the MIMAS simulation for the year 2009. Supersaturation ($S > 1$) is needed to allow the existence of ice whereas $S < 1$ will lead to sublimation of ice particles (e.g. Turco et al., 1982). It turns out that most of the time supersaturation exists, only in the afternoon hours the saturation ratio
10 falls below $S = 1$. The July average shows nearly permanently supersaturated conditions throughout the day.

In summary, the diurnal cycles of background temperature and water vapor in the mesopause region show prevailing supersaturated conditions during the core of the PMC season at ALOMAR and drive the tidal variations of ice parameters.

6 Latitudinal variations

Our numerical simulations indicate that the local time variations of PMC are subject to significant latitudinal dependencies.
15 Figure 8 shows modeled IWC values over latitude for selected local times in July $2007 - 2013$. No threshold was applied so that the median values include 'zero' PMC events. While at 6 LT IWC increases nearly linearly from $60°$N to $84°$N, the slopes are quite different throughout the rest of the day. This indicates that the phase of the local time behavior changes with latitude. As an example, the time of IWC maximum changes from the morning hours at mid latitudes to midnight hours at high latitudes.

Atmospheric
Chemistry
and Physics
Discussions

Latitude band	$\frac{A_{24}}{A_{12}}$	$\frac{A_{24}}{A_8}$	max/min
$61.5-64.5°$N	7.6	6.0	12.6
$67.5-70.5°$N	2.2	4.1	18.3
$73.5-76.5°$N	2.1	4.8	10.4
$79.5-82.5°$N	2.7	7.8	6.9

Table 2. Ratios of IWC tidal amplitudes for July 2009 and different latitudes bands. The ratios of maximum to minimum IWC indicate the variability throughout the day. For details see text.

Figure 9 shows this phase variation in more detail for different latitude bands. It turns out that (1) the amplitude of the local time dependence increases in absolute IWC values towards the pole, (2) the ratio of maximum to minimum IWC decreases towards the pole (see Table 2), and (3) a slight phase shift can be seen with decreasing latitude: the IWC maximum around midnight near $81°$N moves forward in time to 4 LT near $63°$N.

IWC median values at mid latitudes are much smaller (about 100 times) than those at high latitudes. Therefore we also use the ratio of daily maximum to minimum IWC values as an additional indicator for local time variations, see Table 2. Please note that the ratios are calculated from median IWC values without any lower threshold, hence the occurrence frequency has a large influence on the median value. This is in particular important at the lowest latitude band ($61.5-64.5°$N) where rather small PMC occurrence frequencies are modeled. E.g., assuming an IWC threshold of 5 g/km^2, the PMC occurrence frequency at this latitude band is only in the order of $5-10$ % during July whereas moving poleward it increases to about 50 % at $67.5-70.5°$N and 100 % at $79.5-82.5°$N. For this reason the lowest latitude band is omitted in further discussions.

Table 2 also includes tidal amplitude ratios obtained from fitting of 24 h, 12 h, and 8 h harmonic components. We find that for the three highest latitude bands the diurnal component is generally about two times larger than the semidiurnal component. This ratio A_{24}/A_{12} seems to be fairly independent of latitude. There exists a terdiurnal component with a strength of about 20 % which decreases in poleward direction. Hence terdiurnal modes represent a significant part in tidal structures of PMC. On average the ratio of daily maximum to minimum IWC values is about 10 and decreases towards the pole.

These results highlight the importance of taking the PMC tidal variation into account when compiling datasets which are distributed over latitude and local time. As a consequence, the comparison of observations having different local time coverage without applying appropriate corrections will likely result into false conclusions.

7 Long-term variations 1979 – 2013

We have analyzed the long-term variation of IWC local time structures in the period $1979-2013$. Figure 10 shows time series of July mean amplitudes and amplitude ratios for the 24 h and 12 h components in the latitude band $67.5-70.5°$N. The time series feature substantial year-to-year variations of up to 100 % from one year to the next, which is comparable to observations of tidal amplitudes in PMC parameters at ALOMAR (Fiedler et al., 2011). The diurnal component dominates during all years and its amplitude is about twice as much compared to the semidiurnal component. Both amplitude time series are highly

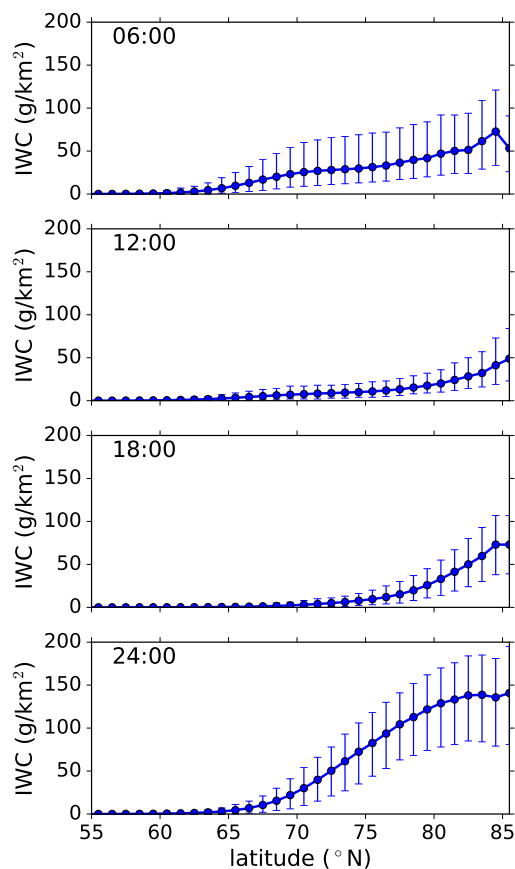**Figure 8.** Median IWC values for July 2007 – 2013 as function of latitude for different local times. The vertical bars represent the lower and upper quartile of the data.

correlated (r = 0.97). IWC values increase by a factor of about 3.8 over the entire time period, however, this increase originates mainly from the years after 1999. The result matches the break point used for trend calculations in the SBUV PMC data set and accounts for a reversal in temperature trend at 83 km (Lübken et al., 2009; DeLand and Thomas, 2015). From linear regression analysis follow slopes of 3.4 and 1.4 g/km^2/dec for the diurnal and semidiurnal amplitude, respectively, over the entire time period 1979 – 2013. The ratio of diurnal to semidiurnal amplitudes remains almost constant in time with some variability. Interestingly the diurnal and semidiurnal phases in IWC (not shown) remain quite constant over the years.

In summary our MIMAS results show a long-term change in tidal amplitudes of IWC. They increase significantly which is presumably caused by an increase of tidal amplitudes of background temperatures during this time period. However, this topic will be subject of future simulations with LIMA/MIMAS.
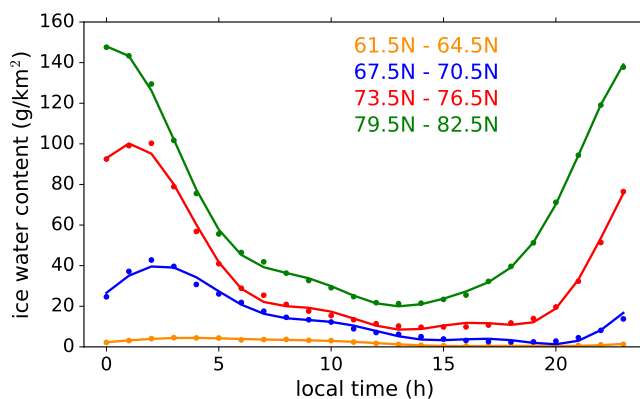
15

Figure 9. Diurnal variation of hourly median IWC values for July 2007 – 2013 for different latitude bands. Dots indicate the data and solid lines are harmonic fits using periods of 24, 12, 8 h.
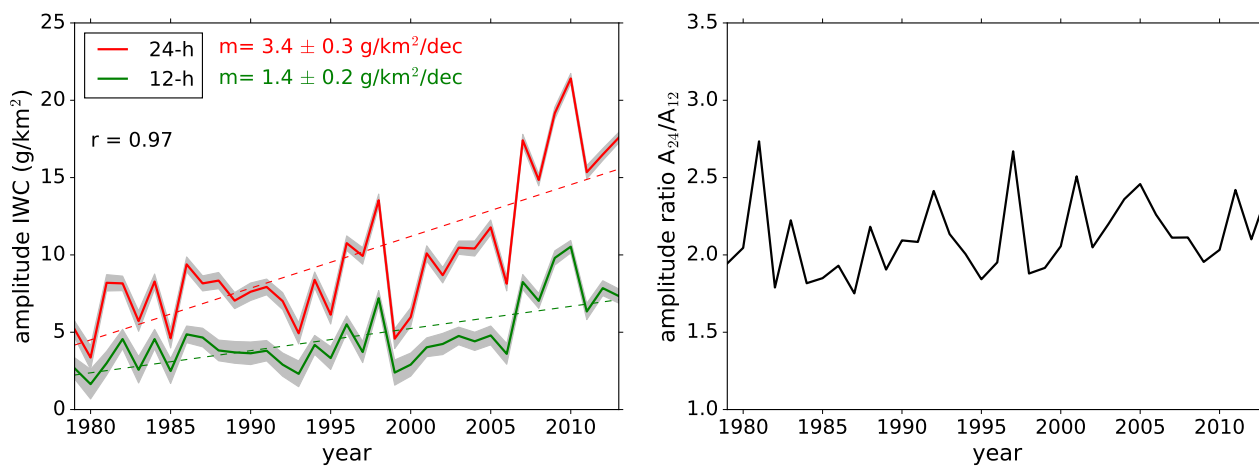

Figure 10. Year-to-year variations of mean values of amplitudes (left) and amplitude ratios (right) for 24-h (red) and 12-h (green) variations of IWC in the time period 1979 – 2013 (July) for the latitude band 67.5 – 70.5°N. The grey areas show error standard deviation of the data set. Dotted lines show the slopes calculated by linear regression.

Atmospheric
Chemistry
and Physics
Discussions

8   Conclusions

In this paper we presented a detailed investigation of tidal effects on PMC occurrence, altitude, brightness and microphysical properties of ice particles as calculated by the MIMAS model. As already discussed in several publications, the interpretation of PMC observations requires a careful treatment of the local time of the observations even for the investigation of long-term

5   records (Fiedler et al., 2011; Stevens et al., 2010; DeLand and Thomas, 2015). We have compared our results to observations by ground-based lidar as well as satellite instruments and find a good agreement when taking into account instrumental sensitivity and local time dependence of observations. MIMAS reproduces the local time variations seen by lidar especially well in the core of the PMC season. In general diurnal, semidiurnal and terdiurnal components contribute to the tidal behavior of PMC parameters calculated by MIMAS.

10   The MIMAS simulations of PMC at ALOMAR show that the brightness varies throughout the day by up to a factor of 7 while the occurrence frequency varies by a factor of 2 to 16 for faint and strong clouds, respectively. The median number density varies by a factor of 2 and the particle radius only by about 30 %. All quantities show the maximum around a local time of 3 ± 2 h. At the same latitude band the time of maximum IWC is about 3 LT and the minimum is found around 18 LT. Without thresholding the data, hourly IWC median values vary by a factor of 10 throughout the diurnal cycle in July (2007 – 2013).

15   Our analysis shows that the local time dependence becomes most evident when concentrating on one single season. When limiting the analysis to the season 2009 we find that the variation of temperature and water vapor at the altitude of brightest PMC (strong cloud class) throughout the day is 2 K and 2 ppmv, respectively. At the altitude of sublimation (about 81.5 km) we find a variation of 2 K and 3 ppmv between minimum and maximum. These variations lead to a change of the saturation ratio from about 1.8 around midnight to 1 in the afternoon.

20   We find that the local time dependence of IWC is affected by latitude. Amplitudes increase towards the pole, but the ratio of daily maximum to minimum values decreases towards the pole. On average the IWC varies by a factor of 10 throughout the diurnal cycle. It is remarkable that the local time of maximum IWC changes from about 4 to 0 LT for latitudes from 63°N to 81°N, respectively.

PMC tidal amplitudes show substantial year-to-year variations as well as a mean increase from 1979 – 2013. The linear trend

25   terms of diurnal and semidiurnal components are calculated to be 3.4 and 1.4 g/km^2/dec. Phases of both tidal components are fairly constant over the whole data set.

It should be noted that gravity waves could mask the influence of tides especially for the terdiurnal component and the year-to-year variations (Thayer et al., 2003). Gravity waves are partly included in the LIMA model, but a detailed investigation regarding their effects on the tidal behavior of PMC is beyond the scope of this paper. However, we expect that the latitudinal

30   and the year-to-year variations of the tidal amplitudes are robust and will help interpreting long-term observations with varying latitudes and fixed or variable local times.

Atmospheric
Chemistry
and Physics
Discussions

Atmospheric
Chemistry
and Physics
Discussions

References

Baumgarten, G., Fiedler, J., Lübken, F.-J., and von Cossart, G.: Particle properties and water content of noctilucent clouds and their interannual variation, Journal of Geophysical Research: Atmospheres, 113, doi:10.1029/2007JD008884, http://dx.doi.org/10.1029/2007JD008884, d06203, 2008.

5 Berger, U.: Modeling of middle atmosphere dynamics with LIMA, Journal of Atmospheric and Solar-Terrestrial Physics, 70, 1170 – 1200, doi:http://dx.doi.org/10.1016/j.jastp.2008.02.004, http://www.sciencedirect.com/science/article/pii/S1364682608000515, 2008.

Berger, U. and Lübken, F.-J.: Trends in mesospheric ice layers in the Northern Hemisphere during 1961 – 2013, Journal of Geophysical Research: Atmospheres, 120, 11,277–11,298, doi:10.1002/2015JD023355, http://dx.doi.org/10.1002/2015JD023355, 2015JD023355, 2015.

10 Berger, U. and von Zahn, U.: Icy particles in the summer mesopause region: Three-dimensional modeling of their environment and two-dimensional modeling of their transport, Journal of Geophysical Research, 107(A11), doi:doi:10.1029/2001JA000316, 2002.

Berger, U. and von Zahn, U.: 3d-Modeling of the trajectories of visible NLC particles indicates that these particles nucleate well below the mesopause., Journal of Geophysical Research, doi:10.1029/2006/JD008106, 2007.

Chu, X., Gardner, C. S., and Roble, R. G.: Lidar studies of interannual, seasonal, and diurnal variations of polar mesospheric clouds at the
15 South Pole, Journal of Geophysical Research: Atmospheres, 108, doi:10.1029/2002JD002524, http://dx.doi.org/10.1029/2002JD002524, 8447, 2003.

Chu, X., Espy, P. J., Nott, G. J., Diettrich, J. C., and Gardner, C. S.: Polar mesospheric clouds observed by an iron Boltzmann lidar at Rothera (67.5S, 68.0W), Antarctica from 2002 to 2005: Properties and implications, Journal of Geophysical Research: Atmospheres, 111, doi:10.1029/2006JD007086, http://dx.doi.org/10.1029/2006JD007086, d20213, 2006.

20 DeLand, M. T. and Thomas, G. E.: Updated PMC trends derived from SBUV data, Journal of Geophysical Research: Atmospheres, 120, 2140–2166, doi:10.1002/2014JD022253, http://dx.doi.org/10.1002/2014JD022253, 2014JD022253, 2015.

DeLand, M. T., Shettle, E. P., Thomas, G. E., and Olivero, J. J.: Direct observations of PMC local time variations by Aura OMI, Journal of Atmospheric and Solar-Terrestrial Physics, 73, 2049 – 2064, doi:http://dx.doi.org/10.1016/j.jastp.2010.11.019, http://www.sciencedirect.com/science/article/pii/S1364682610003512, layered Phenomena in the Mesopause Region, 2011.

25 Fiedler, J., Baumgarten, G., and von Cossart, G.: Noctilucent Clouds above ALOMAR between 1997 and 2001: Occurrence and Properties, Journal of Geophysical Research, 108, 8453, doi:10.1029/2002JD002419, 2003.

Fiedler, J., Baumgarten, G., and von Cossart, G.: Mean diurnal variations of noctilucent clouds during 7 years of lidar observations at ALOMAR, Annales Geophysicae, 23, 1175–1181, doi:10.5194/angeo-23-1175-2005, http://www.ann-geophys.net/23/1175/2005/, 2005.

Fiedler, J., Baumgarten, G., and Lübken, F.-J.: NLC observations during one solar cycle above ALOMAR, Journal of Atmospheric and
30 Solar-Terrestrial Physics, 71, 424 – 433, doi:http://dx.doi.org/10.1016/j.jastp.2008.11.010, http://www.sciencedirect.com/science/article/pii/S1364682608003647, global Perspectives on the Aeronomy of the Summer Mesopause RegionEighth International Workshop on Layered Phenomena in the Mesopause Region, 2009.

Fiedler, J., Baumgarten, G., Berger, U., Hoffmann, P., Kaifler, N., and Lübken, F.-J.: NLC and the background atmosphere above ALOMAR, Atmospheric Chemistry and Physics, 11, 5701–5717, doi:10.5194/acp-11-5701-2011, http://www.atmos-chem-phys.net/11/5701/2011/,
35 2011.

Atmospheric
Chemistry
and Physics
Discussions

Fiedler, J., Baumgarten, G., Berger, U., and Lübken, F.-J.: Long-term variations of noctilucent clouds at ALOMAR, Journal of Atmospheric and Solar-Terrestrial Physics, pp. –, doi:http://dx.doi.org/10.1016/j.jastp.2016.08.006, http://www.sciencedirect.com/science/article/pii/S1364682616302024, 2016.

Gadsden, M. and Schröder, W.: Noctilucent Clouds, vol. 18, Springer-Verlag, New York, lanzerotti, L.J. and Hill, Murray and Stöffler, D., 1998.

Gerding, M., Kopp, M., Hoffmann, P., Höffner, J., and Lübken, F.-J.: Diurnal variations of midlatitude NLC parameters observed by daylight-capable lidar and their relation to ambient parameters, Geophysical Research Letters, 40, 6390–6394, doi:10.1002/2013GL057955, 2013.

Hartogh, P., Sonnemann, G. R., Song Li, Grygalashvyly, M., Berger, U., and Lübken, F.-J.: Water vapor measurements at ALOMAR over a solar cycle compared with model calculations by LIMA, Journal of Geophysical Research: Atmospheres, 115, D00I17, doi:10.1029/2009JD012364, 2010.

Herbort, F., Baumgarten, G., Berger, U., Fiedler, J., Hoffmann, P., and Lübken, F.-J.: Tidal structures within the LIMA model, Advances in Space Research, 40, 802–808, doi:10.1016/j.asr.2007.04.061, 2007.

Hervig, M. E. and Stevens, M. H.: Interpreting the 35 year SBUV PMC record with SOFIE observations, Journal of Geophysical Research: Atmospheres, 119, 12,689–12,705, doi:10.1002/2014JD021923, http://dx.doi.org/10.1002/2014JD021923, 2014JD021923, 2014.

Hervig, M. E., Gordley, L. L., Stevens, M. H., III, J. M. R., Bailey, S. M., and Baumgarten, G.: Interpretation of SOFIE PMC measurements: Cloud identification and derivation of mass density, particle shape, and particle size, Journal of Atmospheric and Solar-Terrestrial Physics, 71, 316 – 330, doi:http://dx.doi.org/10.1016/j.jastp.2008.07.009, http://www.sciencedirect.com/science/article/pii/S1364682608002046, global Perspectives on the Aeronomy of the Summer Mesopause RegionEighth International Workshop on Layered Phenomena in the Mesopause Region, 2009a.

Hervig, M. E., Stevens, M. H., Gordley, L. L., Deaver, L. E., Russell, J. M., and Bailey, S. M.: Relationships between polar mesospheric clouds, temperature, and water vapor from Solar Occultation for Ice Experiment (SOFIE) observations, Journal of Geophysical Research: Atmospheres, 114, doi:10.1029/2009JD012302, http://dx.doi.org/10.1029/2009JD012302, d20203, 2009b.

Hervig, M. E., Siskind, D. E., Stevens, M. H., and Deaver, L. E.: Inter-hemispheric comparison of PMCs and their environment from SOFIE observations, Journal of Atmospheric and Solar-Terrestrial Physics, 104, 285–298, doi:10.1016/j.jastp.2012.10.013, 2013.

Hervig, M. E., Berger, U., and Siskind, D. E.: Decadal variability in PMCs and implications for changing temperature and water vapor in the upper mesosphere, Journal of Geophysical Research: Atmospheres, 121, 2383–2392, doi:10.1002/2015JD024439, http://dx.doi.org/10.1002/2015JD024439, 2015JD024439, 2016.

Jesse, O.: Die Höhe der leuchtenden Nachtwolken, Astronomische Nachrichten, 140, 161, doi:10.1002/asna.18961401102, 1896.

Kiliani, J.: 3-D modeling of noctilucent cloud evolution and relationship to the ambient atmosphere, Ph.D. thesis, IAP Kühlungsborn, Germany, 2014.

Kiliani, J., Baumgarten, G., Lübken, F.-J., Berger, U., and Hoffmann, P.: Temporal and spatial characteristics of the formation of strong noctilucent clouds, Journal of Atmospheric and Solar-Terrestrial Physics, 104, 151 – 166, doi:http://dx.doi.org/10.1016/j.jastp.2013.01.005, http://www.sciencedirect.com/science/article/pii/S1364682613000291, 2013.

Kiliani, J., Baumgarten, G., Lübken, F.-J., and Berger, U.: Impact of particle shape on the morphology of noctilucent clouds, Atmospheric Chemistry & Physics, 15, 12 897–12 907, doi:10.5194/acp-15-12897-2015, 2015.

Lübken, F.-J.: Thermal structure of the Arctic summer mesosphere, Journal of Geophysical Research: Atmospheres, 104, 9135–9149, doi:10.1029/1999JD900076, http://dx.doi.org/10.1029/1999JD900076, 1999.

Atmospheric
Chemistry
and Physics
Discussions

Lübken, F.-J., Baumgarten, G., Fiedler, J., Gerding, M., Höffner, J., and Berger, U.: Seasonal and latitudinal variation of noctilucent cloud altitudes, Geophysical Research Letters, 35, doi:10.1029/2007GL032281, http://dx.doi.org/10.1029/2007GL032281, l06801, 2008.

Lübken, F.-J., Berger, U., and Baumgarten, G.: Stratospheric and solar cycle effects on long-term variability of mesospheric ice clouds, J. Geophys. Res., D00I06, doi:10.1029/2009JD012377, 2009.

5 Lübken, F.-J., Berger, U., and Baumgarten, G.: Temperature trends in the midlatitude summer mesosphere, Journal of Geophysical Research: Atmospheres, 118, 13,347–13,360, doi:10.1002/2013JD020576, http://dx.doi.org/10.1002/2013JD020576, 2013.

Lumpe, J., Bailey, S., Carstens, J., Randall, C., Rusch, D., Thomas, G., Nielsen, K., Jeppesen, C., McClintock, W., Merkel, A., Riesberg, L., Templeman, B., Baumgarten, G., and III, J. R.: Retrieval of polar mesospheric cloud properties from CIPS: Algorithm description, error analysis and cloud detection sensitivity, Journal of Atmospheric and Solar-Terrestrial Physics, 104, 167 – 196, 10 doi:http://dx.doi.org/10.1016/j.jastp.2013.06.007, http://www.sciencedirect.com/science/article/pii/S1364682613001831, 2013.

Megner, L.: Minimal impact of condensation nuclei characteristics on observable Mesospheric ice properties, Journal of Atmospheric and Solar-Terrestrial Physics, 73, 2184 – 2191, doi:http://dx.doi.org/10.1016/j.jastp.2010.08.006, http://www.sciencedirect.com/science/article/pii/S1364682610002397, layered Phenomena in the Mesopause Region, 2011.

Russell, J. M., Bailey, S. M., Gordley, L. L., Rusch, D. W., Horányi, M., Hervig, M. E., Thomas, G. E., Randall, C. E., Siskind, D. E., 15 Stevens, M. H., Summers, M. E., Taylor, M. J., Englert, C. R., Espy, P. J., McClintock, W. E., and Merkel, A. W.: The Aeronomy of Ice in the Mesosphere (AIM) mission: Overview and early science results, Journal of Atmospheric and Solar-Terrestrial Physics, 71, 289 – 299, doi:http://dx.doi.org/10.1016/j.jastp.2008.08.011, http://www.sciencedirect.com/science/article/pii/S1364682608002204, global Perspectives on the Aeronomy of the Summer Mesopause RegionEighth International Workshop on Layered Phenomena in the Mesopause Region, 2009.

20 Russell, J. M., Rong, P., Hervig, M. E., Siskind, D. E., Stevens, M. H., Bailey, S. M., and Gumbel, J.: Analysis of northern midlatitude noctilucent cloud occurrences using satellite data and modeling, Journal of Geophysical Research: Atmospheres, 119, 3238–3250, doi:10.1002/2013JD021017, http://dx.doi.org/10.1002/2013JD021017, 2013JD021017, 2014.

Stevens, M. H., Englert, C. R., DeLand, M. T., and Hervig, M.: The polar mesospheric cloud mass in the Arctic summer, Journal of Geophysical Research: Space Physics, 110, doi:10.1029/2004JA010566, http://dx.doi.org/10.1029/2004JA010566, a02306, 2005.

25 Stevens, M. H., Siskind, D. E., Eckermann, S. D., Coy, L., McCormack, J. P., Englert, C. R., Hoppel, K. W., Nielsen, K., Kochenash, A. J., Hervig, M. E., Randall, C. E., Lumpe, J., Bailey, S. M., Rapp, M., and Hoffmann, P.: Tidally induced variations of polar mesospheric cloud altitudes and ice water content using a data assimilation system, Journal of Geophysical Research: Atmospheres, 115, doi:10.1029/2009JD013225, http://dx.doi.org/10.1029/2009JD013225, d18209, 2010.

Thayer, J. P., Rapp, M., Gerrard, A. J., Gudmundsson, E., and Kane, T. J.: Gravity-wave influences on Arctic mesospheric clouds as deter- 30 mined by a Rayleigh lidar at Sondrestrom, Greenland, Journal of Geophysical Research: Atmospheres, 108, doi:10.1029/2002JD002363, http://dx.doi.org/10.1029/2002JD002363, 8449, 2003.

Thomas, G.: Is the polar mesosphere the miner's canary of global change?, Advances in Space Research, 18, 149 – 158, doi:http://dx.doi.org/10.1016/0273-1177(95)00855-9, http://www.sciencedirect.com/science/article/pii/0273117795008559, 1996.

Thomas, G. E. and Olivero, J. J.: Climatology of polar mesospheric clouds. II - Further analysis of Solar Mesosphere Explorer data, Journal 35 of Geophysical Research: Atmospheres, 94, 14 673–14 681, doi:10.1029/JD094iD12p14673, 1989.

Thomas, G. E., McPeters, R. D., and Jensen, E. J.: Satellite observations of polar mesospheric clouds by the solar backscattered ultraviolet spectral radiometer: Evidence of a solar cycle dependence, Journal of Geophysical Research: Atmospheres, 96, 927–939, doi:10.1029/90JD02312, http://dx.doi.org/10.1029/90JD02312, 1991.

Atmospheric
Chemistry
and Physics
Discussions

Turco, R., Toon, O., Whitten, R., Keesee, R., and Hollenbach, D.: Noctilucent clouds: Simulation studies of their genesis, properties and global influences, Planetary and Space Science, 30, 1147 – 1181, doi:http://dx.doi.org/10.1016/0032-0633(82)90126-X, http://www.sciencedirect.com/science/article/pii/003206338290126X, 1982.

von Zahn, U. and Berger, U.: Persistent ice cloud in the midsummer upper mesosphere at high latitudes: Three-dimensional modeling and cloud interactions with ambient water vapor, Journal of Geophysical Research: Atmospheres, 108, doi:10.1029/2002JD002409, http://dx.doi.org/10.1029/2002JD002409, 8451, 2003.

von Zahn, U., von Cossart, G., Fiedler, J., and Rees, D.: Tidal variations of noctilucent clouds measured at 69N latitude by groundbased lidar, Geophysical Research Letters, 25, 1289–1292, 1998.

Witt, G.: Height, structure and displacements of noctilucent clouds, Tellus, 14, 1–18, doi:10.1111/j.2153-3490.1962.tb00115.x, http://dx.doi.org/10.1111/j.2153-3490.1962.tb00115.x, 1962.